SF2A 2014
J. Ballet, F. Bournaud, F. Martins, R. Monier and C. Reylé (eds)

TRACING PDR PROPERTIES AND STRUCTURE IN THE CLOSEST MASSIVE LOW METALLICITY STAR-FORMING REGION: 30 DORADUS IN THE LMC

M. Chevance[1], S. Madden[1], V. Lebouteiller[1], L. Carlson[2], D. Cormier[3], F. Galliano[1], M.-Y. Lee[1] and R. Wu[4]

Abstract. More complete knowledge of galaxy evolution requires understanding the process of star formation and interaction between the interstellar radiation field and the ISM in galactic environments traversing a wide range of physical parameter space. Here we focus on the impact of star formation on the surrounding low metallicity ISM. Indeed, lowering the metal abundance, as is the case of some galaxies of the early universe, results in an overall lower galactic dust reservoir, hence, less shielding for the formation of the molecular gas necessary for star formation to proceed. A convenient laboratory to zoom into the various phases of the ISM to study the effects of low metallicity on the ISM properties, is our nearest neighbor, the Large Magellanic Cloud, which has a metallicity 1/2 that of solar. The goal is to construct a comprehensive, self-consistent picture of the density, radiation field, and ISM structure in the vicinity of one of the most massive star clusters in our local neighborhood, R136.

Keywords: ISM: individual objects (30 Doradus nebula) – Magellanic Clouds – ISM: structure

1 Introduction

We present *Herschel* spectroscopic data of 30 Doradus (hereafter 30Dor) in the Large Magellanic Cloud (LMC), one of the most active star forming region in our local universe. At a distance of only 50 kpc (Walker 2011), the LMC allows us to have a high spatial resolution view in a low metallicity environment ($\sim 1/2$ solar ; Rolleston et al. 2002; Pagel 2003). We investigate the consequences of reduced metallicity on the heating and cooling mechanisms of the gas, particularly in the photo-dissociation regions (PDRs) where the chemistry and thermal balance are regulated by far-ultraviolet photons (6eV$< h\nu <$13.6eV). In particular, the transition C^+/C/CO can be altered from what we see in galactic regions (Kaufman et al. 1999) and the value of the conversion factor of CO to H_2, the X factor, can be affected. We interpret our observations of the 30Dor region with a PDR model to deduce the physical parameters and the structure of the gas around the massive stellar cluster R136.

2 Observations

2.1 PACS spectoscopy data

We have mapped the five fine structure lines, [CII] 157 μm, [NII] 122 μm, [OI] 63 μm, [OI] 145 μm and [OIII] 88 μm using the PACS spectrometer (Poglitsch et al. 2010) on board *Herschel*. These observations are part of the *Herschel* key program, SHINNING (P.I. E. Sturm), described in Madden et al. (2013), and OT2 (Indebetouw et al.). The different layers of the gas from the highly ionized medium near the star cluster R136, and deeper into the molecular gas can be identified in Fig. 1

The PACS array is composed of 5×5 spatial pixels, covering a total field of view of $47''$. A region of approximately $4' \times 5'$ of 30Dor (~ 56 pc $\times 70$ pc) was covered by *Herschel*, with a resolution of $9.5''$ to $12''$. The data reduction is done with the *Herschel* Interactive Processing Environment (HIPE) v12.0.0 (Ott 2010) from Level 0 to Level 1 and then with PACSman v3.61 (Lebouteiller et al. 2012) to fit the lines and make the maps.

[1] Laboratoire AIM, CEA Saclay, 91191 Gif-sur-Yvette, France
[2] Leiden Observatory, Leiden, Netherlands
[3] Institut für theoretische Astrophysik, Zentrum für Astronomie der Universität Heidelberg, D-69120 Heidelberg, Germany
[4] Department of Astronomy, Graduate School of Science, University of Tokyo, Tokyo, Japan

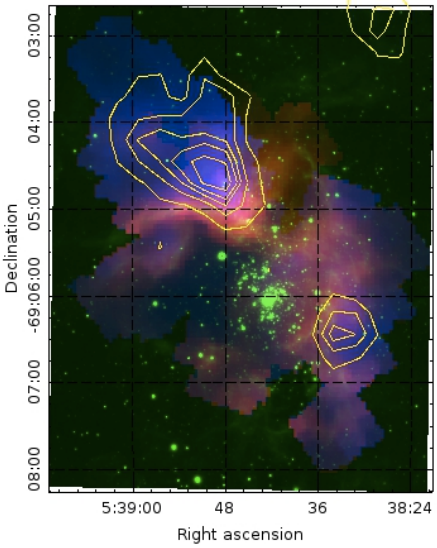

Fig. 1. Three-color image of the 30 Doradus nebula. Red: PACS [OIII] 88 μm. Blue: PACS [CII] 157 μm. Green: VISTA J band. Yellow contours: ^{12}CO(3-2) emission observed with ASTE (Minamidani et al. 2011).

As all of these tracers have different ionization energies and different critical densities, at this resolution we can distinguish different layers of the ionization and neutral structure. We note that the [OIII] emission is very extended, peaks closer to the star cluster than the [CII] emission and is everywhere brighter than [CII] 157 by a factor of 3 to 60. Both [OI] emission lines are PDR tracers and follow the emission of [CII]. The [NII] map is much smaller than the others since the line is very faint, often almost 10 times lower than [CII], but the signal to noise ratio is still larger than 6 everywhere on the map. All the maps are convolved to the resolution of PACS at 160 μm (12.3″), using the kernels from Aniano et al. (2011).

2.2 SPIRE FTS data

The SPIRE instrument includes an Imaging Fourier Transform Spectrometer (FTS) covering the 194-671 μm bandwidth. The [NII] 205 μm and [CI] 370 and 609 μm emission lines were observed in 30Dor with intermediate sampling. The data reduction is described in Lee et al. (in prep).

CO transitions from J = 4 – 3 to J = 13 – 12, also observed in 30Dor, are presented in Lee et al. (in prep).

2.3 Photometry data

PDR models explain the correlations observed between the energy emerging in the FIR cooling lines and the infrared continuum from dust. We use PACS and SPIRE photometry data to derive the total infrared luminosity. PACS and SPIRE maps of the Large Magellanic Cloud at 100, 160 250, 350 and 500 μm were first published in Meixner et al. (2013) as part of the HERITAGE project. We also use the *Spitzer* observations of 30Dor at 24 and 70 μm presented in Indebetouw et al. (2009) to construct the spectral energy distribution (SED).

We have applied the dust SED model of Galliano et al. (2011) to the *Spitzer* MIPS and *Herschel* PACS and SPIRE photometry to explain the observed continuum and to derive the L_{FIR}.

3 Tracing the PDRs

[NII] is a tracer of the low excitation diffuse gas. The critical densities for [NII] 122 μm and [NII] 205 μm are 310 cm^{-3} and 50 cm^{-3} respectively, making the ratio [NII] 122/[NII] 205 a good density tracer. We determine the density using the ratio of [NII] 122/[NII] 205 and the theoretical curve from Bernard-Salas et al. (2012) (Fig. 2). The calculated density ranges from 100 to 600 cm^{-3}. These values are consistent with the density calculated from the [SIII] 18/[SIII] 33 ratio, although this ratio is normally more sensitive to higher densities due to higher critical densities for the [SIII] lines ($n_{crit} = 1.5 \times 10^4$ cm^{-3} for [SiII] 18 μm and $n_{crit} = 4.1 \times 10^3$ cm^{-3} for [SiII] 33 μm).

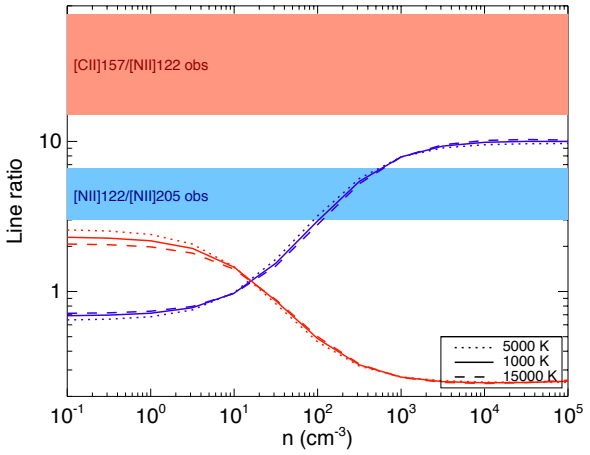

Fig. 2. Theoretical ratios [NII] 122 μm /[NII] 205 μm (blue) and [CII] 157 μm /[NII] 122 μm (red) at temperature 5000 K (dotted line), 10000 K (solid line) and 15000 K (dashed line). Blue and red areas indicate the observed values for the [NII] 122 μm /[NII] 205 μm and the [CII] 157 μm /[NII] 122 μm ratios respectively.

The range of density we find across 30Dor implies a theoretical ratio in the ionized gas of [CII] 157/[NII] 122 $\sim 0.3 - 0.5$ (Fig. 2). However, the observed ratio is significantly higher than this theoretical ratio in the ionized gas, indicating that most of [CII] is emitted in PDRs. At least 80% of the [CII] 157 is expected to be emitted from PDRs in this region. The [CII] emission can be considered a reliable tracer of the PDRs in 30Dor and used as a constraint for the PDR models.

4 PDR modeling

4.1 The Meudon PDR code

Tielens & Hollenbach (1985) showed that the emission from PDRs could be parametrized by the cloud density n and the strength of the UV radiation field illuminating the cloud G_{UV} (in units of the Habing Field, 1.6×10^{-3} ergs cm^{-2} s^{-1}). We use the Meudon PDR code (`http://pdr.obspm.fr/`), describe in Le Petit et al. (2006) to determine these two parameters, using the observational constraints described earlier. This model computes the atomic and molecular structure of interstellar clouds. It considers a 1D stationary plane parallel slab of gas and dust illuminated by a radiation field (from UV to radio) originating from one side of the cloud. The radiative transfer is solved in an iterative way at each point of the cloud as well as absorption by gas and dust and scattering and emission by dust.

We compute a grid of models with a density range from 10^2 to 10^5 cm^{-3} and an incident UV radiation field from 1 to 10^4 on one side (and fixed to 1 on the other side). We fixed the metallicity to half-solar and the total extinction of the cloud to $A_{V,tot} = 30$. We run a constant density model.

4.2 Results

Fig. 3 (left panel) presents the values of G_{UV} and n that reproduce the observed values for the ratios $\frac{[OI]145+[CII]157}{L_{FIR}}$, $\frac{[OI]145}{[CII]157}$, $\frac{[CI]370}{[CI]609}$ and $\frac{[OI]63}{[CII]157}$ for each of the $30'' \times 30''$ pixel of the map of 30Dor. The best solutions for the incident radiation field G_{UV} and the density n, are determined by the minimum of the χ^2 distribution: $\chi^2 = \sum_{i=1}^{N} \frac{D_i(x,y)-M_i}{\sigma_i(x,y)}$, where $D_i(x,y)$ is the observed value of the ratio i for a given pixel (x,y), $\sigma_i(x,y)$ is the uncertainty on this observed ratio and M_i is the value predicted by the model for the ratio i. N is the number of constrains (independent ratios) that are used. The best n and G_{UV} maps are presented on Fig. 3 (middle and right pannels).

The ratio $\frac{[OI]63}{[CII]157}$ is not used as a constraint with the other ratios, due to the fact that [OI] 63 μm can be optically thick (Tielens & Hollenbach 1985; Abel et al. 2007) or can be subject to absorption by cold gas on the line of sight (Liseau et al. 2006).

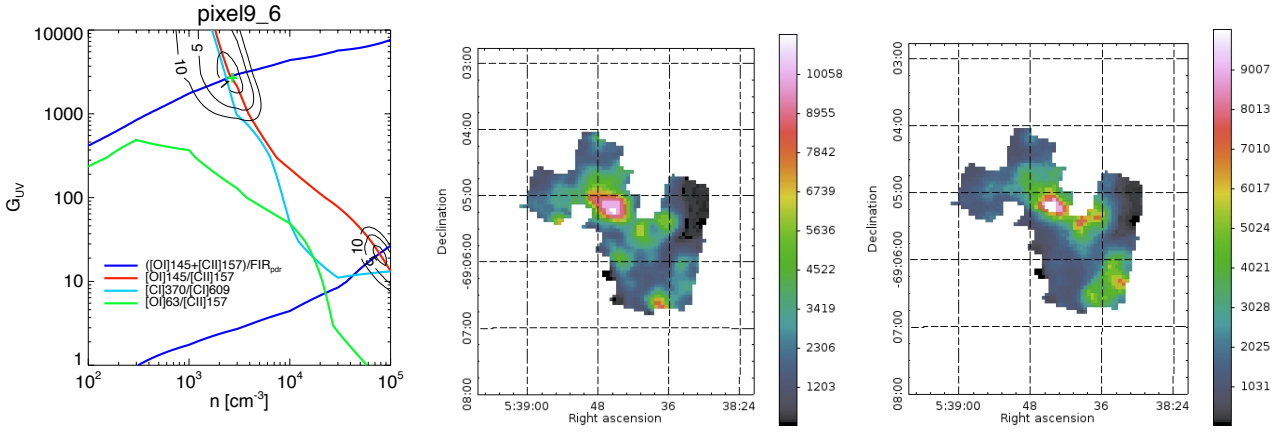

Fig. 3. Left: In colors, contour plot showing the sets of parameters G_{UV} and n able to reproduce the observed values of the ratios $\frac{[OI]145+[CII]157}{L_{FIR}}$ (dark blue), $\frac{[OI]145}{[CII]157}$ (red), $\frac{[CI]370}{[CI]609}$ (light blue) and $\frac{[OI]63}{[CII]157}$ (green). The black contours represent the values of the χ^2 . **Middle:** Best density map (in cm^{-3}) of the 30 Doradus region calculated from a chi square model, using ([OI]145+[CII]157)/ L_{FIR} and [OI]145/[CII]157 as constraints. **Right:** Same, for the incident radiation field G_{UV} (in units of the Habing field).

5 Conclusions

We used *Herschel* PACS and SPIRE observations to constrain a PDR model and determine the physical parameters of the gas in the 30 Doradus region in the LMC. We find a range of densities of $\sim 10^3 - 10^4$ cm and a range of incident radiation field $G_{UV} \sim 10^3 - 10^4$ with the Meudon PDR code.

We find that the ratios of lines that are not co-spatial (such as [CII]/[CI] or [CII]/CO) are not consistent with these solutions . For example, the observed values of the ratios [CII]/CO 1-0 and [CII]/CO 3-2 are much higher than the values predicted by the model. We can explain that by a lower total extinction of the cloud. This will be described in Chevance et al. (in prep).

References

Abel, N. P., Sarma, A. P., Troland, T. H., & Ferland, G. J. 2007, The Astrophysical Journal, 662, 1024

Aniano, G., Draine, B. T., Gordon, K., & Sandstrom, K. M. 2011, Publications of the Astronomical Society of the Pacific, 123, 1218

Bernard-Salas, J., Habart, E., Arab, H., et al. 2012, Astronomy & Astrophysics, 538, A37

Galliano, F., Hony, S., Bernard, J.-P., et al. 2011, Astronomy & Astrophysics, 536, A88

Indebetouw, R., de Messières, G. E., Madden, S. C., et al. 2009, The Astrophysical Journal, 694, 32

Kaufman, M. J., Wolfire, M. G., Hollenbach, D. J., & Luhman, M. L. 1999, ApJ, 527, 795

Le Petit, F., Nehme, C., Le Bourlot, J., & Roueff, E. 2006, The Astrophysical Journal Supplement Series, 164, 506

Lebouteiller, V., Cormier, D., Madden, S. C., et al. 2012, Astronomy & Astrophysics, 548, A91

Liseau, R., Justtanont, K., & Tielens, A. G. G. M. 2006, Astronomy and Astrophysics, 446, 561

Madden, S. C., Rémy-Ruyer, A., Galametz, M., et al. 2013, Publications of the Astronomical Society of the Pacific, 125, 600

Meixner, M., Panuzzo, P., Roman-Duval, J., et al. 2013, The Astronomical Journal, 146, 62

Ott, S. 2010, Astronomical Data Analysis Software and Systems XIX, 434, 139

Pagel, B. E. J. 2003, in Astronomical Society of the Pacific Conference Series, Vol. 304, CNO in the Universe, ed. C. Charbonnel, D. Schaerer, & G. Meynet, 187

Poglitsch, A., Waelkens, C., Geis, N., et al. 2010, Astronomy and Astrophysics, 518, L2

Rolleston, W. R. J., Trundle, C., & Dufton, P. L. 2002, Astronomy and Astrophysics, 396, 53

Tielens, a. G. G. M. & Hollenbach, D. J. 1985, The Astrophysical Journal

Walker, A. R. 2011, Astrophysics and Space Science, 341, 43